Contents lists available at https://www.goldenlightpublish.com/journals/jseam/1-toc

Journal of Structural Engineering & Applied Mechanics

Journal homepage: https://www.goldenlightpublish.com/journals/1/jseam

Golden ratio optimization integrated with quadratic approximation regulated by Lévy flight for structural optimization

Ali Mortazavi[1,*], Erdinç Sarıbaş[1]

[1] İzmir Democracy University, Department of Civil Engineering, İzmir, Türkiye

[*] Corresponding author: A. Mortazavi (ali.mortazavi@idu.edu.tr)

https://doi.org/10.31462/jseam.2026.658

Received 22 December 2025; Revised ---; Accepted 12 February 2026; Available online 30 March 2026

Keywords

Golden ratio optimization
Quadratic approximation
Lévy flight
Structural optimization

Abstract

This study presents a novel Golden Ratio Optimization (GRO) algorithm integrated with Quadratic Approximation (QA) and Lévy Flight (LF) mechanisms to enhance global search efficiency and solution accuracy in structural optimization problems. The proposed method employs the golden ratio principle to guide search balance between exploration and exploitation, while the quadratic approximation model locally estimates the objective landscape to refine candidate solutions. The Lévy flight mechanism introduces adaptive random perturbations to prevent premature convergence and improve diversity within the population. The integrated approach is tested on benchmark truss optimization problems considering stress, displacement, and buckling constraints. Results demonstrate that the proposed method achieves superior convergence speed and robustness compared to conventional metaheuristic algorithms, providing lighter and more efficient structural designs. The findings highlight the potential of the proposed approach as a reliable tool for solving complex structural optimization problems.

1. Introduction

Generally, structural optimization presents several inherent difficulties due to the complex nature of these engineering design problems. These problems often involve high-dimensional and nonlinear objective functions with numerous local minima, making it challenging for algorithms to consistently locate the global optimum [1-6]. Additionally, multiple design constraints such as stress, displacement, and buckling limits introduce discontinuities and nonconvex feasible regions that complicate the search process [7-15]. In some cases, the discrete nature of design variables, such as cross-sectional profiles, further increases computational difficulty. Finally, the computational cost of evaluating structural responses, often requiring repeated finite element analyses, makes metaheuristic optimization both time-consuming and resource-intensive, demanding careful algorithmic tuning and efficiency improvements to achieve practical performance in real-world structural applications [16-23].

The optimization techniques can be divided into two main groups as gradient-based and non-gradient-based approaches [24]. Gradient-based approaches typically require smooth, continuous, and differentiable functions, which are difficult to ensure in problems involving discontinuities, material nonlinearities, or topology changes. In contrast, gradient-free methods like metaheuristic algorithms rely on stochastic search principles rather than gradient information, allowing them to effectively explore irregular and multimodal search spaces [25]. They are also less likely to become trapped in local minima and can handle mixed-variable and highly constrained problems more flexibly. Therefore, despite higher computational costs, metaheuristic algorithms offer greater robustness and adaptability, making them a powerful alternative for solving complex structural optimization problems where traditional methods often fail.

Various methods inspired by diverse sources, such as natural and biological processes, have been introduced in the literature. For example, Tactical flight Optimizer (TFO) models the formation flights of fighter aircrafts during a military mission [26]. Marathon Runner Algorithm (MRA) models the competition behavior between runners in a tournament [27]. Jaya algorithm provides a efficient algorithm based on the balance of good and bad in the real world [28]. Flying Foxes Optimization (FFO) method inspired from the survival strategies of flying foxes during a heatwave [24]. Remora Optimization Algorithm (ROA)

indicates the parasitic behavior of remora [29]. Also, there are several improved versions of these algorithms have been introduced to solve different type of problems for example: Fuzzy reinforced Jaya algorithm that uses a fuzzy decision mechanism to adjust the search behavior of the algorithm [30]. Bayesian Interactive Search Algorithm (BISA) uses a Bayesian regulating module to adjust the algorithm [31]. Hybrid intelligent genetic algorithm (HIGA) combines deep neural networks (DNNs) and genetic algorithms (GAs) in a systematic manner within the optimization process [8]. For a metaheuristic algorithm, achieving a proper balance between exploration and exploitation is critical since excessive exploration leads to slow convergence, while excessive exploitation risks premature convergence to suboptimal designs [32-35]. So, when the balance between exploration and exploitation is properly established in a metaheuristic algorithm, the optimization process becomes significantly more effective and efficient [36-38].

In this regard, to provide an efficient search method, in the current study, the global search capability of the Golden Ratio Algorithm (GRA) is combined with local search ability of the Quadratic Approximation (QA) method. To make a reasonable balance between this to search patterns, a regularization module is developed based on the Lévy flight mechanism. Incorporating the Lévy flight mechanism as a regularization module provides several significant benefits for controlling the exploration and exploitation behavior of a metaheuristic algorithm.

Lévy flight introduces a stochastic step-length distribution characterized by many short moves and occasional long jumps, enabling the algorithm to effectively balance local and global search. The short steps enhance local exploitation, allowing fine-tuning around promising solutions, while the sporadic long jumps promote global exploration, helping the algorithm escape from local minima and explore unexplored regions of the search space. This dynamic movement pattern improves the diversity of candidate solutions and reduces the risk of premature convergence. Furthermore, Lévy-based regularization helps maintain adaptive search intensity, allowing the algorithm to transition naturally from global exploration in early iterations to focused exploitation on later stages. The combined method is tested on suit of structural optimization problems and acquired results are reported and discussed in detail.

The rest of this work is arranged as follows: Section 2 presents the proposed optimization methodology. Section 3 describes the benchmark structural optimization problems and discusses the numerical results and comparative analyses. Section 4 provides a comprehensive discussion based on performance index evaluation and statistical assessment of the algorithms. Finally, Section 5 concludes the paper by summarizing the main findings and outlining directions for future research.

2. Optimization method

In this section, a new optimization technique is presented in detail. Since the method consists of three distinct sub-modules, the details of these modules are first explained, followed by a comprehensive description of the proposed approach. In this regard, Golden Ratio Optimization Method (GROM), Quadratic Approximation Approach (QA) and Lévy flight are described, respectively. Then the proposed hybrid approach is explained comprehensively.

2.1. Golden ratio optimization method

The Golden Ratio Optimization Method (GROM) is a parameter-free metaheuristic algorithm inspired by the natural growth patterns of living organisms that follow the golden ratio (approximately 1.618). This mathematical constant, originally described through the Fibonacci sequence, represents the proportional relationship that appears widely in nature, from plant growth angles to shell spirals, as presented in Fig. 1.

The GROM adopts this natural principle to iteratively refine a population of potential solutions toward an optimal value. The algorithm operates in two main phases. In the first phase, the population's mean vector is evaluated and compared with the least fit solution; if it performs better, it replaces the worst one to accelerate convergence. Then, each solution interacts with a randomly chosen counterpart, and the population mean to generate new candidate solutions guided by the Fibonacci-based update rule. In the second phase, each solution moves closer to the best-performing one and away from the worst, scaled by the inverse of the golden ratio (≈0.618), enhancing local exploitation while maintaining diversity. The two phases of this algorithm are mathematically given as follows:

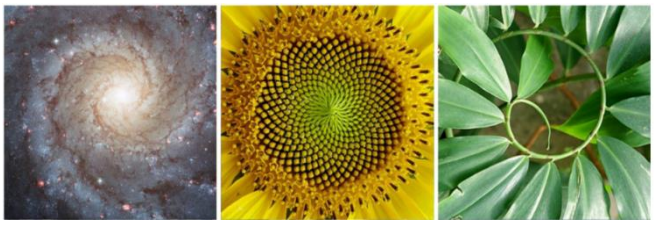

Fig. 1. Golden ratio in nature

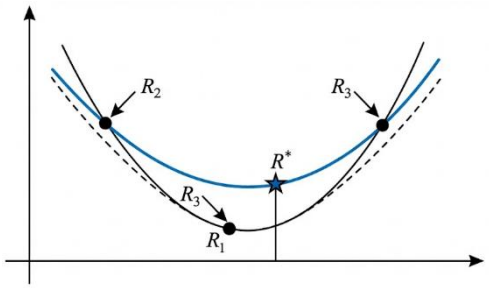

Fig. 2. Schematic view of QA

Phase 1:

$$X_{new} = (1 - F_t) \cdot X_{best} - rand \cdot F_t \cdot X_t \quad (1)$$

Phase 2:

$$X_{new} = X_{old} - \frac{1}{GF} \cdot rand \cdot (X^G_{best} - X^G_{worst}) \quad (2)$$

where,

$$F_t = GF \times \frac{\varphi^T - (1 - \varphi)^T}{\sqrt{5}} \quad (3)$$

in which, GF = 1.618 represents the golden ratio, and T is the iteration rate (t/Tmax).

2.2. Quadratic approximation approach

The Quadratic Approximation (QA) operator identifies the minimum point of a quadratic hypersurface that passes through three positions in a D-dimensional search space. Its procedure can be outlined as follows:

1. Select particle R_1, which has the best objective function value. Then, randomly choose two additional particles, R_2 and R_3, ensuring that at least two among R_1, R_2, and R_3 are distinct.
2. Determine the minimum point R* on the quadratic surface that fits the three points R_1, R_2, and R_3.

The mathematical formulation for this approach is given as follows:

$$R^{new} = 0.5 \frac{(R_2^2 - R_3^2)f(R_1) + (R_3^2 - R_1^2)f(R_2) + (R_1^2 - R_2^2)f(R_3)}{(R_2 - R_3)f(R_1) + (R_3 - R_1)f(R_2) + (R_1 - R_2)f(R_3)} \quad (4)$$

For more clarity the schematic view of the QA approach is presented in Fig. 2.

2.3. Lévy flight

The Lévy flight approach is a stochastic outline widely used in optimization methods to enhance the balance between exploration and exploitation during the search process. As presented in Fig. 3, it is inspired by the random movement patterns observed in nature, particularly in the foraging behavior of animals such as birds, insects, and sharks, where long jumps are occasionally interspersed with short, localized steps. Mathematically, a Lévy flight follows a Lévy distribution, which is a type of heavy-tailed probability distribution. This means that while most steps are relatively small (allowing for fine local search), there is a non-negligible probability of very large steps, which enables the algorithm to escape local optima and explore distant regions of the search space. It is mathematically formulated as follows:

$$\alpha \oplus levy(\beta) \sim \alpha \frac{u}{v^{\frac{1}{\beta}}}, \quad u \sim N(0, \sigma_u^2), \quad v \sim N(0, \sigma_v^2),$$

$$\sigma_u = \left[\frac{\Gamma(1+\beta) \sin\left(\frac{\pi\beta}{2}\right)}{\Gamma\left(\frac{1+\beta}{2}\right) \beta \, 2^{\frac{\beta-1}{2}}} \right]^{\frac{1}{\beta}}, \quad \sigma_v = 1 \quad (5)$$

Here, $\oplus$ denotes the Hadamard product, $\Gamma = \int_0^\infty t^{z-1} e^{-z} \, dt$ is the gamma function, u and v values are obtained from normal distributions, and $\beta \in [1,2]$.

2.4. Upgraded GROM with QA and Lévy flight

In this section, an enhanced search algorithm, referred to as the Upgraded Golden Ratio Optimization Method (UGROM), is presented. The original GROM updates the population's positions based on arithmetic operations. However, in optimization problems with non-convex search domains, such as many structural optimization tasks, the mean position of the entire population may not necessarily yield a better solution than other agents. Moreover, this average point can sometimes fall within an infeasible region of the search space, reducing the algorithm's overall efficiency. Therefore, in this study, an auxiliary vector is generated using the Quadratic Approximation (QA) method instead of a simple arithmetic mean, enabling the population update to account for the nonlinear relationships among its members. Indeed, Quadratic Approximation (QA) as a powerful technique can significantly improve the search capability of the method by injecting local search intelligence and accelerated convergence. It acts as a smart intensification step, guiding the search more efficiently than random mutation or crossover alone.

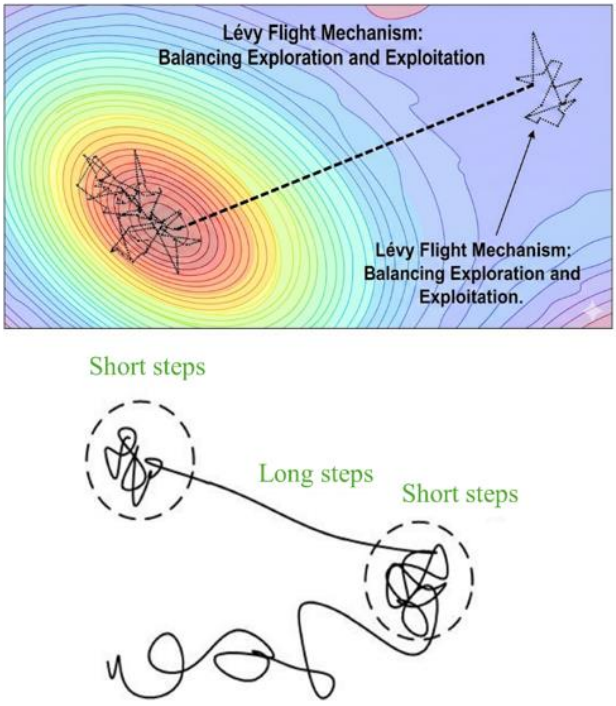

Fig. 3. Schematic presentation of Lévy flight mechanism

The performance of the proposed algorithm depends as much on balancing exploration and exploitation as on the effectiveness of each behavior individually. To achieve this balance in the UGROM module, we incorporate the Lévy flight mechanism. This integration enhances the algorithm's search efficiency by dynamically regulating the trade-off between global exploration and local exploitation. The Lévy distribution enables agents to perform mostly short, local steps combined with occasional long jumps, allowing the algorithm to effectively escape local optima and explore new regions of the search space. This dynamic movement pattern accelerates convergence toward the global optimum while maintaining population diversity. Moreover, Lévy flights increase robustness across different types of complex and high-dimensional problems, offering these benefits without adding extra control parameters, thus preserving the simplicity of the algorithm's structure.

Based on the given facts the first phase of the GROM is modified using quadratic approximation (QA) and therefore, instead of a simple arithmetic mean, an auxiliary vector is generated using the QA method, considering the nonlinear relationships among the members for updating the population. So, the phase of the proposed UGROM is formulated as follows:

Phase 1:

$$X_{co} = 0.5\,\frac{(R_2^2 - R_3^2)f(R_1) + (R_3^2 - R_1^2)f(R_2) + (R_1^2 - R_2^2)f(R_3)}{(R_2 - R_3)f(R_1) + (R_3 - R_1)f(R_2) + (R_1 - R_2)f(R_3)}$$
$$X_t = X_{co} - X_{worst} \qquad \text{if } f(X_{co}) \le f(X_{worst})$$
$$X_{new} = (1 - F_t)X_{best} - rand \cdot F_t X_t \qquad \text{if } f(X_{co}) > f(X_{worst}) \tag{6}$$

where, X_{co} represents the auxiliary vector and its terms are described in Eq. 3; $f(x)$ returns the objective value for any desired agent in the population. Based on this new formulation if the X_{co} is better than X_{worst} it provides a compulsive effect and if not, it provides repulsive effect. In this formulation the rest of the terms are the same as defined previously.

To prevent the algorithm from always converging directly to the best solution, a Lévy flight mechanism is implemented. This helps avoid premature convergence caused by overemphasizing the population's best agent. So, the second phase of the algorithm is modified as follows:

Phase 2:

$$X_{new} = X_{old} + \frac{1}{GF} \cdot \alpha \oplus levy(\beta) \tag{7}$$

where,

$$levy(\beta) \sim \frac{u}{v^{\frac{1}{\beta}}}\,(X_{worst}^{G} - X_{best}^{G}),$$
$$u \sim N(0, \sigma_u^2), \quad v \sim N(0, \sigma_v^2),$$
$$\sigma_u = \left[\frac{\Gamma(1+\beta)\sin\left(\frac{\pi\beta}{2}\right)}{\Gamma\left(\frac{1+\beta}{2}\right)\beta\, 2^{\frac{\beta-1}{2}}}\right]^{\frac{1}{\beta}}, \quad \sigma_v = 1, \quad \beta \in [1,2] \tag{8}$$

where, $\alpha = 0.01$ and $\Gamma = \int_0^\infty t^{z-1}e^{-z}\,dt$ is the gamma function. In the next section the proposed algorithm is tested on suite of numeric problems and the results are discussed.

To provide more clarity on the proposed hybrid methodology and its overall workflow, a schematic representation is presented in Fig. 4.

3. Numerical test

The proposed method is investigated on solving various structural optimization problems with different characteristics. Accordingly, its problem-solving capability is evaluated and compared with those of existing methods reported in the technical literature.

3.1. 18-bar planar truss structure (size and shape)

This benchmark problem illustrates a case of simultaneous size and shape optimization. The schematic configuration of the 18-bar structure is depicted in Fig. 5, and its defining parameters are summarized in Table 1.

Using the developed optimization algorithm, the optimal values for this problem were obtained. The comparative results against other algorithms are presented in Table 2, while the optimal structure, since the problem also involves shape optimization, is illustrated in Fig. 6. The findings show that the proposed algorithm delivers highly accurate solutions and demonstrates superior performance relative to the competing methods. Furthermore, the standard deviation (Std.) obtained from the statistical analysis confirms that the method maintains a highly stable behavior throughout the optimization process. In addition, the number of objective function evaluations indicates that UGROM reaches the optimal solution more rapidly. Overall, these results demonstrate that UGROM achieves a more accurate, more stable, and faster optimization process than the other algorithms. This also implies that the integrated QA and Lévy modules operate synergistically within the GRO framework, effectively reducing unnecessary iterations.

3.2. 25-bar spatial truss structure (size and shape)

The 25-bar spatial truss structure, which is subject to both size and shape optimization, is schematized in Fig. 7. The elements can be grouped into eight categories: (1) A1, (2) A2–5, (3) A6–9, (4) A10–11, (5) A12–13, (6) A14–17, (7) A18–21, and (8) A22–25. The characteristics of this problem are provided in Table 3.

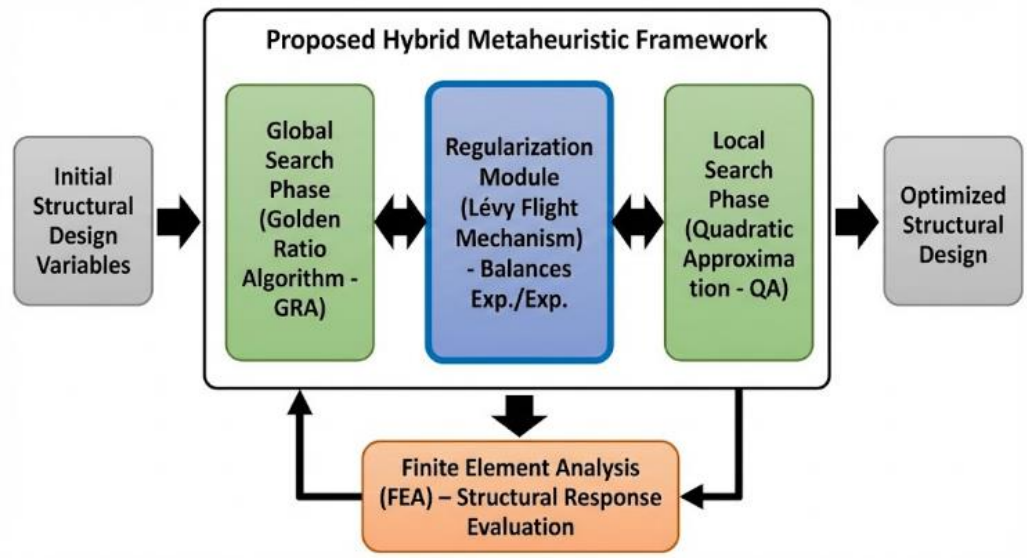

Fig. 4. Overall flowchart of the proposed hybrid methodology framework

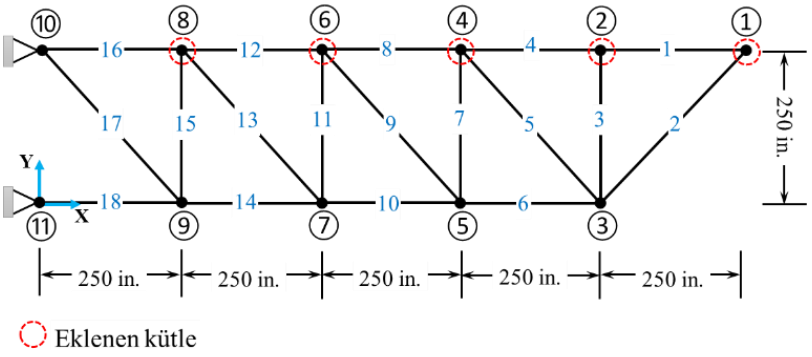

Fig. 5. 18-bar planar truss structure

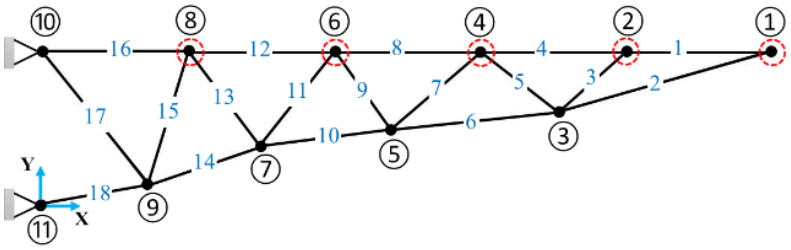

Fig. 6. Optimal design of the 18-bar planar truss structure

Table 1. Description of the 18-bar planar truss structure problem

Property	Description	Value
Design Parameters	Modul of Elasticity	68947.5728 MPa (10 Msi)
	Density	2768 kg/m³ (0.1 lb/in³)
Design Constraints	Allowable compressive stress	137.8951 MPa (20 ksi)
	Allowable tensile stress	137.8951 MPa (20 ksi)
Design Variables	Size	S = {2.0, 2.25, …, 21.5, 2175} in²
	Shape	-571.5 cm (-225 in) ≤ Y_3, Y_5, Y_7, Y_9 ≤ 622.3 cm (245 in) 1968.5 cm (775 in) ≤ X_3 ≤ 3111.5 cm (1225 in) 1333.5 cm (525 in) ≤ X_5 ≤ 2349.5 cm (925 in) 698.5 cm (275 in) ≤ X_7 ≤ 1841.5 cm (725 in) 63.5 cm (25 in) ≤ X_9 ≤ 1206.5 cm (475 in)
Design Load	In the negative Y-direction at nodes 1, 2, 4, 6, and 8	10 ksi

Table 2. Optimal results of the 18-bar planar truss structure system

Size Variables (in^2)	Optimal cross-section					
	HS [39]	GA [40]	TLBO [41]	iPSO [42]	GRO	UGROM
A_1	12.65	12.75	12.25	14.25	12.25	12.50
A_2	17.22	18.50	17.50	11.75	17.50	17.50
A_3	6.17	4.75	5.75	6.00	5.75	5.75
A_4	3.55	3.25	4.25	8.00	4.25	4.25
Shape Variables (in)						
X_3	903.1	917.4475	906.9373	916.4975	906.9373	907.2491
Y_3	174.3	193.7899	179.8866	190.5241	179.8866	179.8671
X_5	630.3	654.3243	637.0087	916.4975	637.0087	636.7873
Y_5	136.3	159.9436	142.617	152.9217	142.6170	141.8271
X_7	402.1	424.4821	408.6414	649.4695	408.6414	407.9442
Y_7	90.5	108.5779	94.1563	105.425	94.1563	94.0559
X_9	195.3	208.4691	199.6503	205.4255	199.6503	198.7897
Y_9	30.6	37.6349	25.3657	36.4252	25.3657	29.5157
Best Weight (lb)	4515.6	4530.7	4528.797	4520.99	4528.796	4512.365
Mean Weight (lb)	-	-	-	4526.585	4531.441	4518.7632
Std. (lb)	-	-	-	14.889	20.2163	13.1150
OFEs	25000	8000	16000	4450	18000	4000

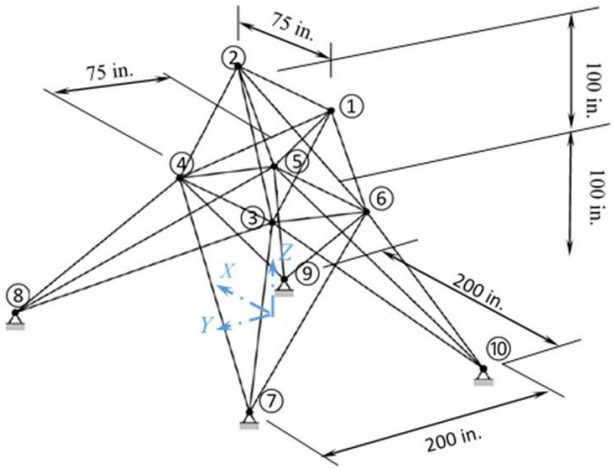

Fig. 7. 25-bar spatial truss structure

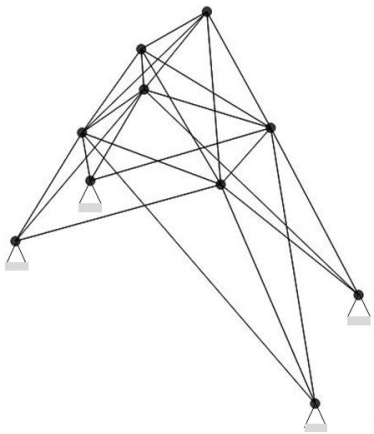

Fig. 8. Optimal design of the 25-bar spatial truss structure

Using the developed optimization algorithm, the optimal values for this problem were obtained. The results, compared with other algorithms, are presented in Table 4. Since this problem also involves shape optimization, the resulting optimal structure is illustrated in Fig. 8. The analysis clearly demonstrates that the proposed algorithm exhibits superior performance compared to the other methods. Statistical data, particularly the standard deviation (Std.), confirm that the algorithm behaves consistently throughout the optimization process. Moreover, the time required to reach the optimal solutions was reduced using the UGROM methodology. These observations indicate that UGROM provides a more accurate, stable, and faster optimization process relative to the other approaches. Furthermore, the synergistic integration of the QA and Lévy modules within the GRO algorithm contributed to minimizing unnecessary iterations. Overall, the results demonstrate that the developed methodology offers significant advantages over alternative algorithms.

3.3. 25-bar spatial truss structure (size)

The spatial 25-element truss structure, which is subject to size optimization, is schematized in Fig. 7. The elements can be grouped into eight categories: (1) A1, (2) A2–5, (3) A6–9, (4) A10–11, (5) A12–13, (6) A14–17, (7) A18–21, and (8) A22–25. This truss is subjected to two loading conditions. The characteristics of the problem are provided in Table 5. Using the developed optimization algorithm, the optimal values for this problem were obtained. The results, compared with other algorithms, are presented in Table 6.

Table 3. Description of the 25-bar spatial truss structure problem

Property	Description	Value
Design Parameters	Modul of Elasticity	68.950 GPa (10^4 ksi)
	Density	2767.990 kg/m³ (0.1 lb/in^3)
Design Constraints	Allowable compressive stress	275.8 MPa (40 ksi)
	Allowable tensile stress	275.8 MPa (40 ksi)
	Allowable Displacement	0.89 mm (0.35 in.)
Design Variables	Size	S = {0.1, 0.2, …, 2.6, 2.8, 3.0, 3.2, 3.4} in.^{2}
	Shape	50.8 cm (20 in.) $\leq X_4 \leq$ 152.4 cm (60 in.) 101.6 cm (40 in.) $\leq X_8 \leq$ 203.2 cm (80 in.) 101.6 cm (40 in.) $\leq Y_4 \leq$ 203.2 cm (80 in.) 254 cm (100 in.) $\leq Y_8 \leq$ 355.6 cm (140 in.) 228.6 cm (90 in.) $\leq Z_4 \leq$ 330.2 cm (130 in.)
Design Load Condition	Node 1	1.0 kip (4.454 kN) in the X-direction 10.0 kip (44.537 kN) in the negative Y-direction 10.0 kip (44.537 kN) in the negative Z-direction.
	Node 2	10.0 kip (44.537 kN) in the negative Y-direction 10.0 kip (44.537 kN) in the negative Z-direction
	Node 3	0.5 kip (2.227 kN) in the X-direction
	Node 6	0.6 kip (2.672 kN) in the X-direction

Table 4. Optimal results of the 25-bar spatial truss structure system

Size Variables (in^2)	Optimal cross-section					
	(GA) [43]	(IGA) [44]	(FM-GA) [45]	(GA) [40]	GRO	UGROM
A_1	0.1	0.1	0.1	0.1	0.1	0.1
A_2	0.2	0.1	0.1	0.1	0.1	0.1
A_3	1.1	1.1	1.1	1.1	1.1	1.0
A_4	0.2	0.1	0.1	0.1	0.1	0.1
A_5	0.3	0.1	0.1	0.1	0.1	0.1
A_6	0.1	0.2	0.1	0.1	0.2	0.1
A_7	0.2	0.2	0.1	0.2	0.2	0.1
A_8	0.9	0.7	1.0	0.8	0.7	0.9
Shape Variables (in.)						
X_4	41.07	35.47	36.23	33.0487	35.47	37.60
Y_4	53.47	60.37	58.56	53.5663	60.37	54.46
Z_4	124.6	129.07	115.59	129.9092	129.07	130.00
X_8	50.8	45.06	46.46	43.7826	45.06	51.89
Y_8	131.48	137.04	127.95	136.8381	137.04	139.55
Best Weight (lb)	136.2	124.94	124.0	120.1149	124.94	117.255
Mean Weight (lb)	-	-	-	-	126.17	118.98
Std. (lb)	-	-	-	-	1.45	1.12
OFEs	-	-	-	-	7100	6400

Table 5. Description of the 25-bar spatial truss structure (size) problem

Property	Description	Value
Design Parameters	Modul of Elasticity	68.950 GPa (10^4 ksi)
	Density	2767.990 kg/m³ (0.1 lb/in³
Design Constraints	Allowable compressive stress	275.8 MPa (40 ksi)
	Allowable tensile stress	275.8 MPa (40 ksi)
	Allowable Displacement	0.89 mm (0.35 in.)
Design Variables	Size	S = [0.0645 cm² (0.01 in²), 21.94 cm² (3.4 in²)]
Design Load Conditions	Condition 1	
	Node 1	1.0 kip (4.454 kN) in the X-direction 10.0 kip (44.537 kN) in the Y-direction 5.0 kip (22.268 kN) in the negative Z-direction
	Node 2	10.0 kip (44.537 kN) in the Y-direction 5.0 kip (22.268 kN) in the negative Z-direction
	Node 3	0.5 kip (2.227 kN) in the X-direction
	Condition 2	
	Node 1	20.0 kip (89.074 kN) in the Y-direction 5.0 kip (22.268 kN) in the negative Z-direction. 20.0 kip (89.074 kN) in the negative Y-direction
	Node 2	5.0 kip (22.268 kN) in the negative Z-direction

Table 6. Optimal results of the 25-bar spatial truss structure (size) system

Size Variables (cm²)	Optimal cross-section					
	PSO [46]	BB-BC [47]	ABC-AP [48]	TLBO [49]	GRO	UGROM
A_1	0.010	0.0100	0.0110	0.0100	0.0100	0.010
A_2-A_5	2.052	2.0920	1.9790	1.9878	1.8308	1.910
A_6-A_9	3.001	2.9640	3.0030	2.9914	3.1834	2.798
A_{10}-A_{11}	0.010	0.0100	0.0100	0.0102	0.0100	0.010
A_{12}-A_{13}	0.010	0.0100	0.0100	0.0100	0.0100	0.010
A_{14}-A_{17}	0.684	0.6890	0.6900	0.6828	0.7017	0.708
A_{18}-A_{21}	1.616	1.6010	1.6790	1.6775	1.7266	1.836
A22 -A25	2.673	2.6860	2.6520	2.6640	2.5713	2.645
Best Weight (kg)	545.21	545.380	545.175	545.175	545.159	545.09
Mean Weight (kg)	546.84	-	-	545.483	545.720	545.301
Std. (kg)	1.478	-	-	0.306	0.512	0.217
OFEs	9596	-	-	12199	10200	8700

The obtained outcomes report the best weight, average weight, standard deviation, and the number of objective function evaluations. These data indicate that the integration of the QA and Lévy modules enhances the algorithm, yielding a more accurate, consistent, and faster optimization process.

3.4. 72-bar spatial truss structure (size)

The problem characteristics of the 72-bar spatial truss structure, which is subject to size optimization and illustrated in Fig. 9, are provided in Table 7. The 72 structural members of this truss are categorized into 16 groups by exploiting symmetry: (1) A1–A4, (2) A5–A12, (3) A13–A16, (4) A17–A18, (5) A19–A22, (6) A23–A30, (7) A31–A34, (8) A35–A36, (9) A37–A40, (10) A41–A48, (11) A49–A52, (12) A53–A54, (13) A55–A58, (14) A59–A66, (15) A67–A70, and (16) A71–A72. Using the developed optimization algorithm, the optimal values for this problem were obtained, and the comparative results against other algorithms are presented in Table 8.

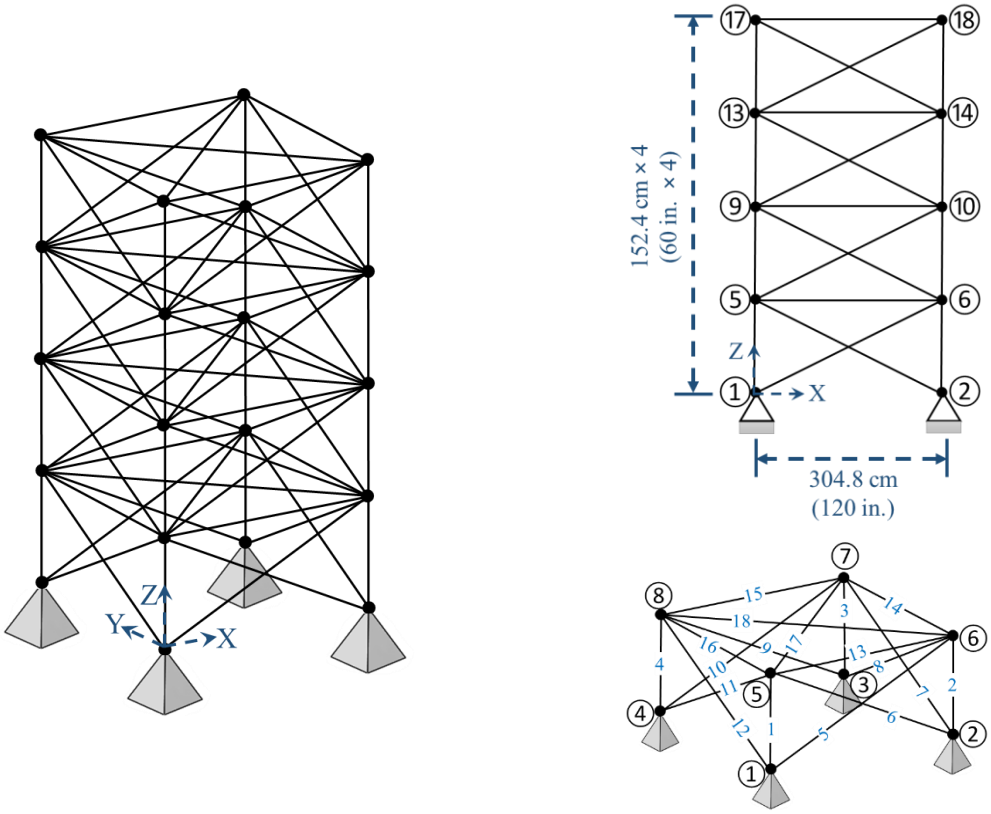

Fig. 9. 72-bar spatial truss structure

Table 7. Description of the 72-bar spatial truss structure (size) problem

Property	Description	Value
Design Parameters	Modul of Elasticity	68.950 GPa (10^4 ksi)
	Density	2767.990 kg/m³ (0.1 lb/in³)
Design Constraints	Allowable compressive stress	172.375 MPa (25 ksi)
	Allowable tensile stress	172.375 MPa (25 ksi)
	Allowable Displacement	0.635 cm (0,25 in)
Design Variables	Size	S =[0.6452 cm² (0.10 in²), 25.81 cm² (4.00 in²)]
Design Load Condition	Condition 1	
	Node 17	5.0 kip (22.268 kN) in the X-direction
		5.0 kip (22.268 kN) in the Y-direction
		5.0 kip (22.268 kN) in the negative Z-direction
	Condition 2	
	Node 17	5.0 kip (22.268 kN) in the negative Z-direction
	Node 18	5.0 kip (22.268 kN) in the negative Z-direction
	Node 19	5.0 kip (22.268 kN) in the negative Z-direction
	Node 20	5.0 kip (22.268 kN) in the negative Z-direction

The outcomes clearly demonstrate the superiority of the proposed algorithm over the other methods. The analysis of the standard deviation (Std.) values confirms the balanced and stable performance of the method throughout the optimization process. The evaluation conducted using the UGROM method further shows that the optimal solutions were achieved in a more efficient manner. These findings reveal that UGROM delivers a more accurate, stable, and faster optimization experience compared with the alternative algorithms. The excellent synergy between the QA and Lévy modules within the GRO framework reinforces these advantages by preventing unnecessary iterations. Overall, the results provide strong evidence that the proposed approach offers a distinct performance advantage over existing methods.

Table 8. Optimal results of the 72-bar spatial truss structure (size) system

Size Variables (in^2)	Optimal cross-section					
	ACO [50]	PSO [46]	BB-BC [47]	WCA [51]	GRO	UGROM
A_1- A_4	1.948	1.7427	1.8577	1.990	1.990	1.83649
A_5- A_{12}	0.508	0.5185	0.5059	0.442	0.563	0.502096
A_{13}- A_{16}	0.101	0.1000	0.1000	0.111	0.111	0.100007
A_{17}- A_{18}	0.102	0.1000	0.1000	0.111	0.111	0.10039
A_{19}- A_{22}	1.303	1.3079	1.2476	1.228	1.228	1.252233
A_{23}- A_{30}	0.511	0.5193	0.5269	0.563	0.442	0.503347
A_{31}- A_{34}	0.101	0.1000	0.1000	0.111	0.111	0.100176
A_{35}- A_{36}	0.100	0.1000	0.1012	0.111	0.111	0.100151
A_{37}- A_{40}	0.561	0.5142	0.5209	0.563	0.563	0.572989
A_{41}- A_{48}	0.492	0.5464	0.5172	0.563	0.563	0.549872
A_{49}- A_{52}	0.100	0.1000	0.1004	0.111	0.111	0.100445
A_{53}- A_{54}	0.107	0.1095	0.1005	0.111	0.111	0.100102
A_{55}- A_{58}	0.156	0.1615	0.1565	0.196	0.196	0.157583
A_{59}- A_{66}	0.550	0.5092	0.5507	0.563	0.563	0.52222
A_{67}- A_{70}	0.390	0.4967	0.3922	0.391	0.391	0.435582
A_{71}- A_{72}	0.592	0.5619	0.5922	0.563	0.563	0.597158
Best Weight (lb)	385.76	381.91	379.85	389.334	389.334	380.4583
Mean Weight (lb)	-	-	382.08	389.941	391.0253	381.9914
Std. (lb)	-	-	1.912	1.430	2.002	1.278
OFEs	-	-	19621	4600	6800	4200

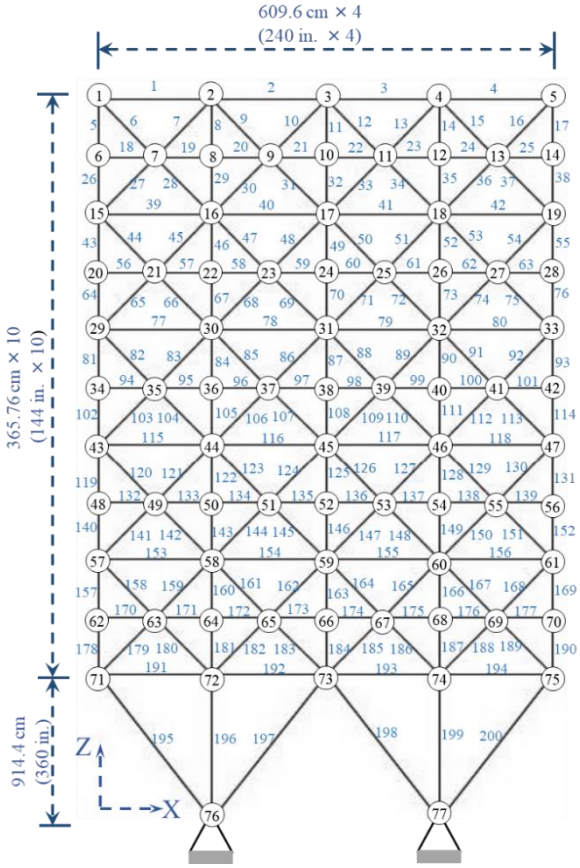

Fig. 10. 200-bar planar truss structure

Table 9. 200-bar planar truss structure grouping

Group	Members
1	1-2-3-4
2	5-8-11-14-17
3	19-20-21-22-23-24
4	18-25-56-63-94-101-132-139-170-177
5	26-29-32-35-38
6	6-7-9-10-12-13-15-16-27-28-30-31-33-34-36-37
7	39-40-41-42
8	43-46-49-52-55
9	57-58-59-60-61-62
10	64-67-70-73-76
11	44-45-47-48-50-51-53-54-65-66-68-69-71-72-74-75
12	77-78-79-80
13	81-84-87-90-93
14	95-96-97-98-99-100
15	102-105-108-111-114
16	82-83-85-86-88-89-91-92-103-104-106-107-109-110-112-113
17	115-116-117-118
18	119-122-125-128-131
19	133-134-135-136-137-138
20	140-143-146-149-152
21	120-121-123-124-126-127-129-130-141-142-144-145-147-148-150-151
22	153-154-155-156
23	157-160-163-166-169
24	171-172-173-174-175-176
25	178-181-184-187-190
26	158-159-161-162-164-165-167-168-179-180-182-183-185-186-188-189
27	191-192-193-194
28	195-197-198-200
29	196-199

3.5. 200-bar planar truss structure (size)

The example considered for size optimization is the 200-bar planar truss shown in Fig. 10. This system is subjected to three loading conditions. The 200 elements of the truss are grouped into 29 categories, as presented in Table 9. The characteristics of the problem are provided in Table 10. Using the developed optimization algorithm, the optimal values for this problem were obtained, and the comparative results against other algorithms are presented in Table 11.

Based on the obtained optimal numerical and statistical results, it is evident that the proposed algorithm exhibits clear superiority over the competing methods. The analysis of the standard deviation (Std.) values demonstrates the stable and consistent performance of the algorithm throughout the optimization process. The results obtained through the UGROM method indicate that the optimal solutions are achieved more efficiently. This provides strong evidence that UGROM offers a more advantageous optimization performance, particularly in terms of accuracy, speed, and stability, compared not only with the other algorithms but also with its baseline version, the GRO method. Notably, the harmonious integration of the QA and Lévy modules within the GRO framework significantly contributes to reducing unnecessary iterations, thereby enhancing the overall efficiency of the method. These findings reveal that the proposed methodology delivers outstanding performance and compatibility relative to existing approaches.

Table 10. Description of the 200-bar planar truss structure (size) problem

Property	Description	Value
Design Parameters	Modul of Elasticity	206.000 MPa (30.000 ksi)
	Density	7933.410 kg/m^3 (0.283 lb/in^3)
Design Constraints	Allowable compressive stress	68.95 MPa (10 ksi)
	Allowable tensile stress	68.95 MPa (10 ksi)
	Allowable Displacement	0.635 cm (0.25 in)
Design Variables	Size	S =[0.10 in^2 (0.6452 cm^2), 20 in^2 (129.03 cm^2)]
Design Load Condition	Condition 1	
	Nodes 1, 6, 15, 20, 29, 43, 48, 57, 62, and 71	1.0 kip (4.45 kN) in the X-direction
	Condition 2	
	Node 1, 2, 3, 4, 5, 6, 8, 10, 12, 14, 15, 16, 17, 18, 19, 20, 22, 24, ..., 71, 72, 73, 74, and 75	10.0 kip (44.5 kN) in the negative Y-direction
	Condition 3	Combination of Condition 1 and Condition 2

Table 11. Optimal results of the 200-bar planar truss structure (size) system

Size Variables (in^2)	Optimal cross-section					
	HS [39]	CMLPSA [52]	FA [33]	iPSO [16]	GRO	UGROM
A_1	0.1253	0.1468	0.1213	0.1460	0.1469	0.1535
A_2	1.0157	0.9400	0.9484	0.9410	0.9447	0.9190
A_3	0.1069	0.1000	0.1081	0.1000	0.1000	0.1200
A_4	0.1096	0.1000	0.1000	0.1010	0.1000	0.1000
A_5	1.9369	1.9400	1.9343	1.9410	1.9405	1.8679
A_6	0.2686	0.2962	0.3014	0.2960	0.2958	0.2936
A_7	0.1042	0.1000	0.2091	0.1000	0.1000	0.1000
A_8	2.9731	3.1042	2.9906	3.1210	3.1040	2.9638
A_9	0.1309	0.1000	0.1042	0.1000	0.1000	0.1000
A_{10}	4.1831	4.1042	4.1351	4.1730	4.1040	3.9428
A_{11}	0.3967	0.4034	0.5124	0.4010	0.4035	0.3725
A_{12}	0.4416	0.1912	0.1614	0.1810	0.1916	0.4502
A_{13}	5.1873	5.4282	4.9798	5.4230	5.4279	4.9604
A_{14}	0.1912	0.1000	0.2003	0.1000	0.1000	1.0761
A_{15}	6.2410	6.4282	6.5128	6.4220	6.4279	5.9759
A_{16}	0.6994	0.5734	0.6719	0.5710	0.5736	0.7817
A_{17}	0.1158	0.1327	0.1405	0.1560	0.1338	0.7389
A_{18}	7.7643	7.9717	8.2108	7.9580	7.9733	7.3811
A_{19}	0.1000	0.1000	0.1005	0.1000	0.1000	0.6649
A_{20}	8.8279	8.9717	7.6314	8.9580	8.9723	8.3014
A_{21}	0.6986	0.7049	0.7011	0.7200	0.7054	1.1908
A_{22}	1.5563	0.4196	1.5139	0.4780	0.4208	0.9125
A_{23}	10.9806	10.8636	11.2394	10.8970	10.8669	10.8197
A_{24}	0.1317	0.1000	0.3391	0.1000	0.1000	0.1000
A_{25}	12.1492	11.8606	12.2394	11.8970	11.8673	11.6979
A_{26}	1.6373	1.0339	1.6851	1.0800	1.0349	1.3886

Table 11. Continued

Size Variables (in^2)	Optimal cross-section					
	HS [39]	CMLPSA [52]	FA [33]	iPSO [16]	GRO	UGROM
A_{27}	5.0032	6.6818	5.0003	6.4620	6.6844	4.9511
A_{28}	9.3545	10.8113	9.8011	10.799	10.8073	8.8128
A_{29}	15.0919	13.8404	14.9249	13.922	13.8448	14.6635
Best Weight (lb)	25447.1	25445.63	25670.01	25488.22	25450.87	25148.30
Mean Weight (lb)	-	-	26020.84	25996.18	26450 21	25952.10
Std. (lb)	-	-	1001.56	101.40	70.31	62.03
OFEs	-	-	12510	15900	16000	12000

4. Discussion

This section presents a comprehensive evaluation of the selected algorithms through a combination of numerical assessments and statistical analyses. Performance index values are computed for each optimization method under consideration. The detailed findings and comparative discussions are provided in the following subsection.

4.1. Performance index analysis

This section introduces a Performance Index (PI) designed to provide a comprehensive evaluation of the selected algorithms. The PI is developed based on the conceptual framework proposed in [53] and aims to quantify an algorithm's effectiveness in solving the problem under consideration. By incorporating multiple performance dimensions, including solution precision, robustness of the search process, and computational efficiency, the PI enables a structured and holistic assessment of algorithmic behavior. The mathematical definition of the proposed index is given as follows:

$$PI = \frac{1}{NP}\sum_{i=1}^{NP}\omega_i P_i \ , \qquad 0 \le \omega_i \le 1 \ \vee \sum_{i=1}^{NC}\omega_i = 1 \tag{9}$$

where, NP denotes the total number of benchmark problems, while NC represents the number of performance metrics considered. The term P_i corresponds to the normalized value of the ith performance indicator. In the present work, algorithmic performance is assessed with respect to three principal criteria: solution accuracy, search robustness, and computational efficiency. Based on these factors, the Comparative Performance Index (PI) for the jth algorithm is formulated as follows:

$$PI_j = \text{normalised}\left(\frac{1}{NP}\sum_{i=1}^{2}\omega_i P_j = \omega_1 \cdot AC_j + \omega_2 \cdot ST_j + \omega_3 \cdot CC_j\right), \quad 0 \le \omega_i \le 1 \ \vee \sum_{i=1}^{NP}\omega_i = 1 \tag{10}$$

In this formulation, AC_j, ST_j, and CC_j denote the accuracy, stability, and computational cost associated with the jth algorithm for the problem under investigation, respectively. The operator normalize(·) refers to the Min–Max normalization procedure. In this study, each algorithm is assessed across three fundamental performance dimensions, accuracy, robustness, and computational efficiency. The corresponding mathematical definitions of the normalized performance measures are provided below:

$$AC_j = \left(1 - \frac{(Mean)_j}{\text{Max}(Mean)}\right), \ ST_j = \left(1 - \frac{(Std.)_j}{\text{Max}(Std.)}\right), \quad CC_j = \left(1 - \frac{(OFEs)_j}{\text{Max}(OFEs)}\right) \tag{11}$$

Table 12 summarizes the computed PI values for the selected algorithms when applied to the considered problems. For additional clarity, Fig. 11 illustrates the performance indices of all algorithms across the four benchmark problems.

Based on the results reported, the Performance Index (PI) analysis provides a clear comparative overview of the effectiveness of the considered optimization algorithms across different structural benchmark problems. Since the PI integrates accuracy, stability, and computational cost into a single metric, higher PI values indicate superior overall performance. For the 18-bar truss problem (size and shape optimization), UGROM achieves the highest PI value (100), demonstrating a well-balanced performance across all evaluated criteria. Among the competing methods, iPSO exhibits relatively strong performance, whereas HS and GRO show noticeably lower PI values, indicating limitations in either solution quality, robustness, or computational efficiency. In the 25-bar truss problem (size and shape optimization), UGROM again outperforms all other algorithms with a PI value of 100. While GA-based variants such as FM-GA and IGA present moderate performance, their PI values remain significantly lower, suggesting that UGROM provides a more consistent trade-off between accuracy and computational demand. A similar trend is observed for the 25-bar truss size optimization problem, where UGROM attains the maximum PI score. Although ABC-AP, TLBO, and GRO show comparable PI values, UGROM maintains a clear advantage, reflecting its

robustness and efficiency even when several algorithms perform competitively. For the more complex 72-bar truss size optimization problem, BB-BC achieves the highest PI value, closely followed by UGROM. This indicates that while UGROM remains highly competitive, certain algorithms may excel under specific problem characteristics. Nevertheless, UGROM still demonstrates strong overall performance, outperforming several well-established methods such as PSO and WCA. Finally, in the large-scale 200-bar truss size optimization problem, UGROM once again achieves the maximum PI value, highlighting its scalability and robustness in handling high-dimensional optimization tasks. Other algorithms exhibit noticeably lower PI values, emphasizing the increased difficulty of maintaining accuracy and stability as problem size grows.

Table 12. The performance index for selected problems solved with considered algorithms

Problem	Method					
18-bar (size and shape)	HS	GA	TLBO	iPSO	GRO	UGROM
	11.403	80.569	42.701	97.654	33.223	100
25-bar (size and shape)	GA	IGA	FM-GA	GA	GRO	UGROM
	22.253	59.454	64.414	84.903	59.454	100
25-bar (size)	PSO	BB-BC	ABC-AP	TLBO	GRO	UGROM
	60	30	80	80	80	100
72-bar (size)	ACO	PSO	BB-BC	WCA	GRO	UGROM
	37.705	100	88.279	20.601	17.827	93.443
200-bar (size)	HS	CMLPSA	FA	iPSO	GRO	UGROM
	42.857	42.857	24.950	34.975	41.872	100

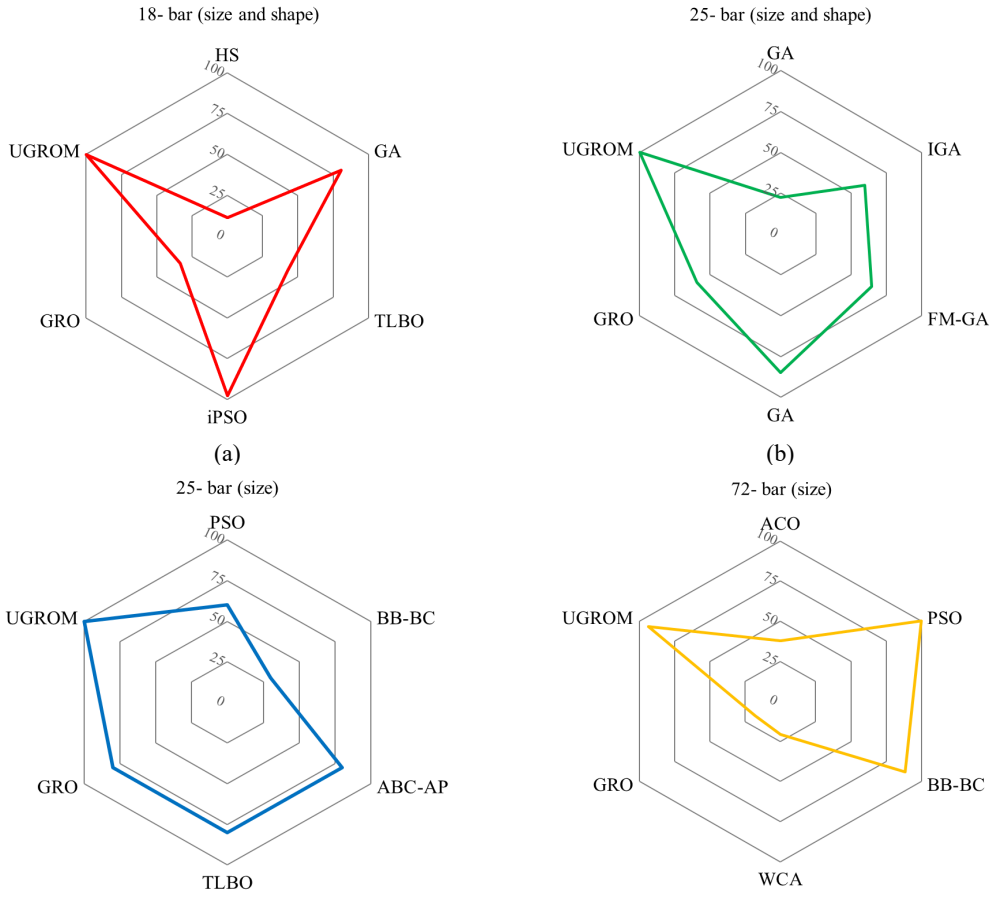

Fig. 11. Performance index for a) 18-bar (size and shape) b) 25-bar (size and shape) c) 25-bar (size) d) 72-bar (size), and e) 200-bar (size)

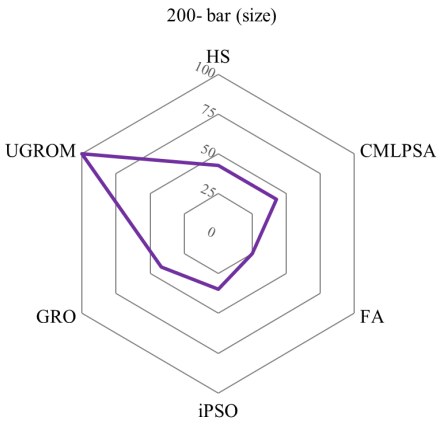

(e)

Fig. 11. Continued

Overall, the PI analysis confirms that UGROM consistently delivers superior or highly competitive performance across a wide range of benchmark problems, particularly in terms of balancing solution accuracy, search stability, and computational efficiency. These results validate the effectiveness and reliability of the proposed algorithm for solving both medium- and large-scale engineering optimization problems.

5. Conclusions

This study proposed an upgraded metaheuristic optimization framework, termed UGROM, by integrating Quadratic Approximation (QA) and Lévy flight (LF) mechanisms into the original Golden Ratio Optimization Method (GROM). The primary objective was to enhance the balance between exploration and exploitation while improving convergence rate, solution accuracy, and robustness in solving complex structural optimization problems.

The incorporation of the QA operator enabled the algorithm to exploit local landscape information more effectively, providing a guided intensification strategy beyond simple population averaging. Meanwhile, the Lévy flight mechanism acted as an adaptive regularization module, introducing controlled stochastic perturbations that enhanced population diversity and prevented premature convergence. Importantly, these improvements are achieved without increasing the number of algorithmic control parameters, thereby preserving the simplicity and practicality of the original GROM framework.

The performance of UGROM was extensively evaluated on a comprehensive suite of benchmark structural optimization problems, including size-only and simultaneous size-shape optimization of planar and spatial truss structures ranging from low- to large-scale systems. Numerical results consistently demonstrated that UGROM outperformed or matched well-established metaheuristic algorithms in terms of optimal structural weight, convergence efficiency, and statistical stability. The reduced standard deviation values and lower numbers of objective function evaluations further confirmed the robustness and computational efficiency of the proposed approach.

In addition, a unified Performance Index (PI) was employed to provide a holistic assessment by simultaneously accounting for solution accuracy, robustness, and computational cost. The PI analysis validated that UGROM delivers superior overall performance across most benchmark problems, particularly for high-dimensional and computationally demanding cases, highlighting its scalability and reliability.

Overall, the results confirm that the synergistic integration of QA and Lévy flight within the GROM framework significantly enhances optimization performance for structural engineering applications. The proposed UGROM algorithm offers a powerful, stable, and efficient tool for solving constrained engineering optimization problems. Future research may focus on extending the method to multi-objective formulations, reliability-based design optimization, and real-world large-scale structural systems, as well as investigating its applicability to other engineering domains.

Declarations

Conflict of interests

The author(s) declared no potential conflicts of interest with respect to the research, authorship, and/or publication of this article.

Funding

This work is supported by the İzmir Democracy University Scientific Research Projects (BAP) under project number TEZ-MHF/2301.

Author contributions

All authors contributed equally to this study. All authors have read and approved the final manuscript and accept equal responsibility for its content.

Data availability statement

The data presented in this study are available on request from the corresponding author.

Use of generative AI and AI-assisted technologies

The author(s) confirm the author(s) did not use any AI tools in the preparation of this work/research/study.

References

[1] Mortazavi A (2022) Interactive fuzzy Bayesian search algorithm: A new reinforced swarm intelligence tested on engineering and mathematical optimization problems. Expert Syst Appl 187:115954.

[2] Zainal NA, Azad S, Zamli KZ (2020) An adaptive fuzzy symbiotic organisms search algorithm and its applications. IEEE Access 8:225384–225406.

[3] Mortazavi A (2020) Large-scale structural optimization using a fuzzy reinforced swarm intelligence algorithm. Adv Eng Softw 142:102790.

[4] Bigham A, Gholizadeh S (2020) Topology optimization of nonlinear single-layer domes by an improved electro-search algorithm and its performance analysis using statistical tests. Struct Multidiscip Optim 62(4):1821–1848.

[5] Moloodpoor M, Mortazavi A (2025) A comparative review of fuzzy reinforced search algorithms: Methods and applications. Arch Comput Methods Eng.

[6] Moloodpoor M, Mortazavi A (2025) Developing surrogate models based on a fuzzy reinforced swarm intelligence and ANN to estimate the performance of parabolic trough collectors. Sol Energy 300:113880.

[7] Mortazavi A, Seker S (2021) Enhanced quadratic approximation integrated with butterfly optimization: A new search algorithm tested on structural and mathematical problems. Rev Constr 20(2):215–235.

[8] Liu J, Xia Y (2022) A hybrid intelligent genetic algorithm for truss optimization based on deep neural network. Swarm Evol Comput 70:101120.

[9] Li Y, Zheng X, Chen C, Wang J, Xu S (2022) Exponential gradient with momentum for online portfolio selection. Expert Syst Appl 187:115889.

[10] Faiella D, Calderoni B, Mele E (2022) Seismic retrofit of existing masonry buildings through inter-story isolation system: A case study and general design criteria. J Earthq Eng 26(4):2051–2087.

[11] Eid HF, Garcia-Hernandez L, Abraham A (2022) Spiral water cycle algorithm for solving multi-objective optimization and truss optimization problems. Eng Comput 38(2):963–973.

[12] Chen Y, Sato D, Miyamoto K, She J (2022) Response-spectrum-based design method for active base-isolated buildings with viscous and hysteretic dampers. Mech Syst Signal Process 180:109413.

[13] Moloodpoor M, Mortazavi A, Özbalta N (2024) Performance assessment of parabolic trough collectors under climatic conditions of Izmir, Türkiye: A case study. [Dergi bilgisi eksik].

[14] Moloodpoor M, Mortazavi A (2024) A new constraint handling approach based on enhanced quadratic approximation: Tested on optimal design of mechanical systems and truss structures. J Eng Technol Appl Sci 9(2):85–112.

[15] Moloodpoor M, Mortazavi A, Özbalta N (2021) Thermo-economic optimization of double-pipe heat exchanger using a compound swarm intelligence. Heat Transfer Res 52(6):1–20.

[16] Mortazavi A, Moloodpoor M (2021) Enhanced butterfly optimization algorithm with a new fuzzy regulator strategy and virtual butterfly concept. Knowl Based Syst 228:107291.

[17] Kaveh A, Biabani Hamedani K, Kamalinejad M (2021) Set theoretical variants of optimization algorithms for system reliability-based design of truss structures. Period Polytech Civ Eng.

[18] Lieu QX, Do DTT, Lee J (2018) An adaptive hybrid evolutionary firefly algorithm for shape and size optimization of truss structures with frequency constraints. Comput Struct 195:99–112.

[19] Ho-Huu V, Nguyen-Thoi T, Truong-Khac T, Le-Anh L, Vo-Duy T (2018) An improved differential evolution based on roulette wheel selection for shape and size optimization of truss structures with frequency constraints. Neural Comput Appl 29(1):167–185.

[20] Mortazavi A, Toğan V (2016) Simultaneous size, shape, and topology optimization of truss structures using integrated particle swarm optimizer. Struct Multidiscip Optim 54(4):715–736.

[21] Mortazavi A, Toğan V, Moloodpoor M (2019) Solution of structural and mathematical optimization problems using a new hybrid swarm intelligence optimization algorithm. Adv Eng Softw 127:106–123.

[22] Moloodpoor M, Mortazavi A (2022) Simultaneous optimization of fuel type and exterior walls insulation attributes for residential buildings using a swarm intelligence. Int J Environ Sci Technol 19:2809–2822.

[23] Moloodpoor M, Mortazavi A (2022) Thermo-economic optimization for saving energy in residential buildings using population-based optimization techniques. J Constr Eng Manag Innov 5(1):45–63.

[24] Zervoudakis K, Tsafarakis S (2022) A global optimizer inspired from the survival strategies of flying foxes. Eng Comput.

[25] Mortazavi A (2019) Comparative assessment of five metaheuristic methods on distinct problems. Dicle Univ J Eng 10(3):879.

[26] Mortazavi A, Moloodpoor M (2025) Tactical flight optimizer: A novel optimization technique tested on mathematical, mechanical, and structural optimization problems. [Dergi bilgisi eksik] 67(2):330–352.

[27] Mortazavi A (2024) Marathon runner algorithm: Theory and application in mathematical, mechanical and structural optimization problems. [Dergi bilgisi eksik].

[28] Rao RV (2019) Jaya: An advanced optimization algorithm and its engineering applications. Springer, Cham.

[29] Jia H, Peng X, Lang C (2021) Remora optimization algorithm. Expert Syst Appl 185:115665.

[30] Mortazavi A (2024) A fuzzy reinforced Jaya algorithm for solving mathematical and structural optimization problems. Soft Comput 28(3):2181–2206.

[31] Mortazavi A (2021) Bayesian interactive search algorithm: A new probabilistic swarm intelligence tested on mathematical and structural optimization problems. Adv Eng Softw 155:102994.

[32] Mortazavi A (2024) A novel type-2 decision mechanism for dynamic parameter adaptation: Theory and application in mathematical and structural problems. Neural Comput Appl.

[33] Mortazavi A, Moloodpoor M (2021) Differential evolution method integrated with a fuzzy decision-making mechanism and virtual mutant agent: Theory and application. Appl Soft Comput 112:107808.

[34] Li W, Meng X, Huang Y, Mahmoodi S (2021) Knowledge-guided multiobjective particle swarm optimization with fusion learning strategies. Complex Intell Syst 7(3):1223–1239.

[35] Sánchez D, Melin P, Castillo O (2020) Comparison of particle swarm optimization variants with fuzzy dynamic parameter adaptation for modular granular neural networks for human recognition. J Intell Fuzzy Syst 38:3229–3252.

[36] Mortazavi A, Toğan V (2017) Sizing and layout design of truss structures under dynamic and static constraints with an integrated particle swarm optimization algorithm. Appl Soft Comput 51:239–252.

[37] Assimi H, Jamali A, Nariman-zadeh N (2017) Sizing and topology optimization of truss structures using genetic programming. Swarm Evol Comput 37:90–103.

[38] Souza RR, Fadel Miguel LF, Lopez RH, Torii AJ, Miguel LFF (2016) A backtracking search algorithm for the simultaneous size, shape and topology optimization of trusses. Lat Am J Solids Struct 13(15):2622–2651.

[39] Lee KS, Geem ZW (2004) A new structural optimization method based on the harmony search algorithm. Comput Struct 82(9):781–798.

[40] Rahami H, Kaveh A, Gholipour Y (2008) Sizing, geometry and topology optimization of trusses via force method and genetic algorithm. Eng Struct 30(9):2360–2369.

[41] Dede T, Ayvaz Y (2015) Combined size and shape optimization of structures with a new meta-heuristic algorithm. Appl Soft Comput 28:250–258.

[42] Mortazavi A, Toğan V, Nuhoğlu A (2017) Weight minimization of truss structures with sizing and layout variables using integrated particle swarm optimizer. J Civ Eng Manag 23(8):985–1001.

[43] Wu SJ, Chow PT (1995) Integrated discrete and configuration optimization of trusses using genetic algorithms. Comput Struct 55(4):695–702.

[44] Wei L, Tang T, Xie X, Shen W (2011) Truss optimization on shape and sizing with frequency constraints based on parallel genetic algorithm. Struct Multidiscip Optim 43(5):665–682.

[45] Kaveh A, Kalatjari V (2004) Size geometry optimization of trusses by the force method and genetic algorithm. J Appl Math Mech 84(5):347–357.

[46] Perez RE, Behdinan K (2007) Particle swarm approach for structural design optimization. Comput Struct 85(19):1579–1588.

[47] Camp CV (2007) Design of space trusses using Big Bang–Big Crunch optimization. J Struct Eng 133(7).

[48] Sonmez M (2011) Artificial bee colony algorithm for optimization of truss structures. Appl Soft Comput 11(2):2406–2418.

[49] Camp CV, Farshchin M (2014) Design of space trusses using modified teaching–learning based optimization. Eng Struct 62–63:87–97.

[50] Camp CV, Bichon BJ (2004) Design of space trusses using ant colony optimization. J Struct Eng 130(5):741–751.

[51] Sadollah A, Eskandar H, Bahreininejad A, Kim JH (2015) Water cycle, mine blast and improved mine blast algorithms for discrete sizing optimization of truss structures. Comput Struct 149:1–16.

[52] Lamberti L (2008) An efficient simulated annealing algorithm for design optimization of truss structures. Comput Struct 86(19):1936–1953.

[53] Bharati (1994) Controlled random search techniques and their applications. University of Roorkee, Roorkee.